Journal of Solid State Chemistry **161,** 152–160 (2001)
doi:10.1006/jssc.2001.9310, available online at http://www.idealibrary.com on IDEAL®

Spinel Solid Solutions in the Li–Fe–Mn–O System

Tomáš Grygar,*,[1] Petr Bezdička,* Petr Vorm,* Neli Jordanova,† and Petr Krtil‡

*Institute of Inorganic Chemistry, Academy of Sciences of CR, 250 68 Řež, Czech Republic; †Institute of Geophysics, Academy of Sciences of CR, Boční II/1401, 141 31 Prague 4, Czech Republic; and ‡J. Heyrovský Institute of Physical Chemistry, Academy of Sciences of CR, Dolejškova 3, 180 00 Prague 8, Czech Republic

Received February 23, 2001; in revised form July 5, 2001; accepted July 12, 2001

The ranges of Li–Fe–Mn composition in which single-phase microparticulate spinel oxides are formed by heating in air were determined. The aim was to reevaluate previously published reports on binary solid solutions between $LiFe_5O_8$ and Li–Mn–O spinels by covering the whole possible range of $(Li, Fe, Mn)_3O_4$ spinels with Mn valence higher than 3. To sensitively detect possible heterogeneity of the elemental distribution or phase composition, chemical and X-ray powder diffraction analyses were used, temperature dependence of magnetic susceptibility was obtained for samples rich in Fe, and electrochemical reductive dissolution was studied by means of voltammetry of microparticles. Instead of a continuous series of solid solutions, three regions were found with different dependence of lattice parameters on elemental composition. A region of nonuniform solid solutions was found at Fe/(Fe+Mn)>0.4 and Mn valence >3.2. © 2001 Academic Press

Key Words: **Li–Fe–Mn–O spinels; solid solution; X-ray diffraction; voltammetry.**

INTRODUCTION

Several Li–Mn–O spinels (1, 2), $LiFe_5O_8$, and their solid solutions were studied in the Li–Fe–Mn–O system, such as $Li_4Mn_5O_{12}$–$LiFe_5O_8$ (3), $LiMn_2O_4$–$LiFe_5O_8$ (4–6), $Li(Fe,Mn)_5O_8$ (3, 7–9), $MnFe_2O_4$–$LiFe_5O_8$ (10), $MnFe_2O_4$–$LiFeMnO_4$ (11), $LiFe_xMn_{2-x}O_4$, $x = 0.5$ (12), and others (13–15) (Fig. 1). These previous studies suggested that spinels can be expected to occur not only as binary but as complex solid solutions of general formula $(Li,Fe,Mn)_3O_4$, but a systematic work in this ternary solid solution has not been published. Additionally, several phenomena observed in the previous reports suggest that the $(Li,Fe,Mn)_3O_4$ plane is not homogeneous but contains some boundaries of varying ideality.

Li–Fe–Mn–O spinels have mostly cubic symmetry $Fd3m$, only Fe-rich spinels exhibit ordering of Li and Fe in octahedral positions leading to the symmetry $P4_332$ (6–10). Li^+ occupies all tetrahedral positions in $LiMn_2O_4$ and $Li_4Mn_5O_{12}$, and is exclusively present in octahedral positions in $LiFe_5O_8$, but in solid solutions $(Li,Fe,Mn)_3O_4$ the Li distribution among tetrahedral and octahedral positions does not follow a simple linear dependence on $Fe/(Fe + Mn)$ ratio (3–5, 9). Deviations from the Vegard law were reported in solid solutions $LiMn_2O_4$–$LiFe_5O_8$ with $Fe/(Fe + Mn) \geq 0.6$ (6), suggesting that the solid solutions deserve a further study.

Li–Mn–O spinels have exceptional electrochemical properties that caused a boom of the interest in their properties in the early 1990s (16, 17). Later in that decade, several Li–M–Mn–O spinels, particularly with stoichiometric formula $Li_2MMn_3O_8$, where M is a first-row transition metal including Fe, attracted the renewed attention of battery electrochemists (12, 18). If Li–Fe–Mn–O spinels were practically used, systematic knowledge about the range of their stability and their ionic distribution would be of a practical importance.

In our previous paper (14), we showed that X-ray diffraction analysis is not sufficiently sensitive to reveal a certain nonuniform elemental distribution in Li–Fe–Mn–O samples, because the ionic radii of Mn^{3+} and Fe^{3+} are too similar. Voltammetry of immobilized microparticles (19) is, however, more sensitive to actual Fe/Mn ratio in spinels and also in other Fe–Mn oxide solid solutions (20). Facility of voltammetry as an analytical tool for characterization of Mn oxides was already proved; reductive electrochemical dissolution (21, 22), H^+ insertion (23), and reversible Li^+ ion insertion (2) were used. This enabled us to test more minutely the quality of a synthetic series of Li–Fe–Mn–O spinels. In this work, we describe the preparation and characterization of Li–Fe–Mn–O spinels that also include compositions other than those of binary solid solutions already reported. The spinels were synthesized by a sol–gel route, uniformity of phase and elemental composition were checked by voltammetry, X-ray powder diffraction, and stoichiometry by chemical analysis. Temperature dependence of magnetic susceptibility was also used to characterize the spinels. The aim of this report was to evaluate the stability of well crystalline Li–Fe–Mn–O spinels in the area $LiFe_5O_8$–$Li(Fe,Mn)_5O_8$–$Li_xMn_{2-x}O_4$.

[1] To whom correspondence should be addressed.

0022-4596/01 $35.00

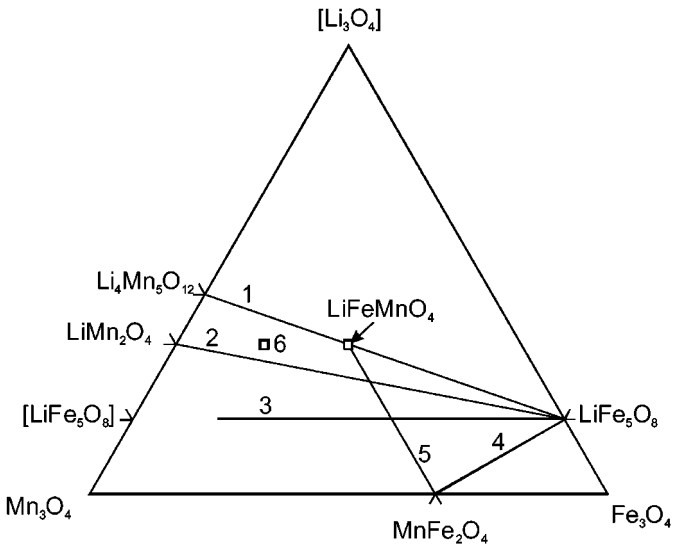

FIG. 1. Solid solutions already described. Hypothetical phases are in square brackets. Lines: 1, Ref. (3); 2, Refs. (4–6); 3, Refs. (3, 7–9); 4, Ref. (10); 5, Ref. (11); point 6: $Li_2FeMn_3O_8$ (12, 18).

EXPERIMENTAL

The samples were synthesized by the sol–gel method described in (21). The solution of corresponding metal nitrates and citric acid in minimal amount of water was evaporated on hot plate to dry foam that was subsequently fired at about 400°C and calcined at the desired temperature (600 to 850°C) in air. The molar amount of citric acid should be equal to or larger than 2/3 of the molar amount of nitrates to avoid possible blaze of the dry foam. The phase purity of spinels was checked by X-ray diffraction, elemental composition by atomic emission (Li) and absorption (Fe, Mn) spectrometry, and Mn valence by permanganometric titration after dissolution in an excess of acidic solution of the Mohr salt. X-ray powder diffraction was performed with a Siemens D5005 (Bruker AXS, Germany) using Cu$K\alpha$ radiation (40 kV, 30 mA) and diffracted beam monochromator. Qualitative analysis was performed with Bede ZDS for Windows, version 1.99 and JCPDS PDF-2 database (24). For quantitative analysis of XRD patterns we used PowderCell for Windows, version 2.3 (25) with structural models based on the ICSD database (26). For Rietveld analysis, Fullprof code was used (27).

Temperature dependence of magnetic susceptibility was obtained by KLY-3 Kappabridge (Geofyzika Brno, Czech Republic). The Curie temperature was obtained from the inflex point estimated by differentiating the χ/T curve.

Electrochemical dissolution was performed by voltammetry in aqueous solution as described in Refs. (14, 20, 21) with potentiostat μAutolab controlled by the GPES 4.4 program (EcoChemie, Utrecht, the Netherlands). Samples were deposited by intensive rubbing of a sample on filter paper with a paraffin-impregnated graphite working electrode. Saturated calomel electrode (SCE) was used as a reference, with a Pt-plate as a counter-electrode. Linear sweep voltammetry was done at 2 mV/s scan rate from open circuit potential to -1.1 V. Deaerated 0.2 M acetic acid–acetate buffer (1:1) was used as supporting electrolyte; measurements were done under N_2 stream to decrease the background current at potentials < 0.5 V vs SCE.

Electrochemical Li^+ insertion reaction was studied in nonaqueous solution as described in Ref. (28) with potentiostat PAR263A. Samples were deposited on the gold electrode by spreading their suspension and heating at 450°C for 45 min. Li/1 M Li^+ was used as a reference electrode and a Pt plate was used as a counter-electrode. $LiN(CF_3SO_2)_2$ in propylene carbonate was used as supporting electrolyte. The experiments were performed in a glove box. Cyclic voltammetric curves were integrated to evaluate the total amount of reversibly inserted extracted Li^+.

RESULTS

The single-phase Li–Fe–Mn–O spinels obtained are summarized in Table 1. Mean error of chemical analyses was about 2%. X-ray diffraction patterns were processed to structure refinement using the Rietveld analysis (15 samples, Table 2) or only to refine the unit cell parameters (16 samples). In Li-rich mixtures, an admixture of monoclinic Li_2MnO_3 was always produced. Significant Li deficiency in compositions close to the vertex of hypothetical spinel $LiMn_5O_8$ led to the formation of tetragonal hausmannite Mn_3O_4 or an unidentified, probably tetragonal phase also observed by Blasse (3). The samples containing admixtures of tetragonal impurities (9 samples) or Li_2MnO_3 (22 samples), and samples containing two cubic spinels (7 samples) were not included in Table 1. The phase composition of all samples of Li–Fe–Mn–O oxides was plotted in triangular in Fig. 2. The results of the linear regression analysis of the dependence of the lattice parameter on the elemental composition are given in Table 3. The regression was performed according to

$$a = A + B^*Fe/(Fe + Mn) + C^*Li/(Fe + Mn). \quad [1]$$

Zero hypothesis (nonsignificant influence of the corresponding independent variable) was evaluated by t-test, and if it was accepted, the corresponding significance level was also included in the table.

Elemental and redox analyses permitted us to calculate the total occupancy of cationic positions assuming a complete occupation of anionic sites. Under such assumption the mean occupancy of cationic sites was 99% ($\sigma = 0.7\%$, $n = 24$, spinels of regions A and B). The low concentration of cationic vacancies is not surprising after crystallization at

TABLE 1
Formulas of the Single Phase Samples Synthesized, the Results of Chemical and X-Ray Diffraction Analyses, and Classification According to Fig. 2

Spinel formula	T/°C	Li/(Fe + Mn)	Fe/(Fe + Mn)	Mn valence	Li(T)/Li(tot)	a/Å	Region
$Li_{0.47}Fe_{0.71}Mn_{1.78}O_4$	850	0.19	0.28	3.03	1.00	8.392	A
$Li_{0.46}Fe_{0.73}Mn_{1.77}O_4$	800	0.18	0.29	3.01	1.00	8.406	A
$Li_{0.54}Fe_{0.71}Mn_{1.71}O_4$	800	0.22	0.29	3.11	1.00	8.379	A
$Li_{0.43}Fe_{1.03}Mn_{1.51}O_4$	850	0.17	0.41	2.96	1.00	8.399	A
$Li_{0.43}Fe_{1.23}Mn_{1.31}O_4$	800	0.17	0.48	2.97	0.87	8.389	A
$Li_{0.43}Fe_{1.20}Mn_{1.28}O_4$	800	0.17	0.48	3.10	0.83	8.379	A
$Li_{0.49}Fe_{1.19}Mn_{1.27}O_4$	800	0.20	0.48	3.08	0.90	8.369	A
$Li_{0.54}Fe_{1.45}Mn_{1.02}O_4$	850	0.22	0.59	3.05	0.63	8.366	A
$Li_{0.54}Fe_{1.71}Mn_{0.76}O_4$	850	0.22	0.69	3.06	0.44	8.352	A
$Li_{0.51}Fe_{2.03}Mn_{0.44}O_4$	850	0.21	0.82	3.20	0.32	8.336	A
$Li_{0.54}Fe_{2.23}Mn_{0.24}O_4$	850	0.22	0.90	3.25	0.07	8.329	A
$Li_{0.90}Fe_{0.16}Mn_{1.88}O_4$	850	0.44	0.08	3.52	1.00	8.247	B
$Li_{0.96}Fe_{0.16}Mn_{1.83}O_4$	850	0.48	0.08	3.58	1.00	8.234	B
$Li_{1.00}Fe_{0.16}Mn_{1.77}O_4$	600	0.52	0.08	3.68	1.00	8.195	B
$Li_{0.94}Fe_{0.37}Mn_{1.70}O_4$	600	0.45	0.18	3.48	1.00	8.259	B
$Li_{0.81}Fe_{0.40}Mn_{1.77}O_4$	850	0.37	0.18	3.39	1.00	8.305	B
$Li_{0.99}Fe_{0.37}Mn_{1.65}O_4$	600	0.49	0.18	3.58	0.99	8.246	B
$Li_{0.66}Fe_{0.43}Mn_{1.85}O_4$	850	0.29	0.19	3.27	1.00	8.309	B
$Li_{0.88}Fe_{0.58}Mn_{1.47}O_4$	600	0.43	0.28	3.66	1.00	8.245	B
$Li_{0.59}Fe_{0.67}Mn_{1.68}O_4$	850	0.25	0.28	3.21	1.00	8.351	B
$Li_{0.80}Fe_{0.62}Mn_{1.52}O_4$	600	0.37	0.29	3.52	1.00	8.262	B
$Li_{0.70}Fe_{0.65}Mn_{1.60}O_4$	850	0.31	0.29	3.35	1.00	8.316	B
$Li_{0.94}Fe_{0.59}Mn_{1.42}O_4$	600	0.47	0.29	3.73	1.00	8.244	B
$Li_{0.78}Fe_{0.84}Mn_{1.34}O_4$	850	0.36	0.38	3.51	1.00	8.293	C
$Li_{0.71}Fe_{0.90}Mn_{1.39}O_4$	850	0.31	0.39	3.40	1.00	8.317	C
$Li_{0.80}Fe_{0.88}Mn_{1.27}O_4$	850	0.37	0.41	3.61	1.00	8.276	C
$Li_{0.61}Fe_{0.96}Mn_{1.38}O_4$	850	0.26	0.41	3.27	1.00	8.318	C
$Li_{0.56}Fe_{1.41}Mn_{0.99}O_4$	850	0.24	0.59	3.25	0.81	8.339	C
$Li_{0.68}Fe_{1.31}Mn_{0.92}O_4$	850	0.31	0.59	3.67		8.34	C
$Li_{0.60}Fe_{2.21}Mn_{0.22}O_4$	850	0.24	0.91	3.46	0.34	8.328	C
$Li_{0.58}Fe_{2.20}Mn_{0.21}O_4$	850	0.24	0.91	3.64	0.34	8.327	C

Note. The formulas were obtained from chemical analysis assuming four O ions per formula unit. Li and Fe valences are assumed to be I and III, respectively. Li(T)/Li(tot) is a fraction of Li in tetrahedral positions. a is spinel lattice parameter ($Fd3m$ or $P4_332$).

temperatures equal to or higher than 600°C. The cation-deficient Li–Mn–O spinels are commonly obtained after calcination at about 400°C, but such specimens have highly defective structure and small mean coherence length. Le Cras *et al.* (1) stated that ordered Li–Mn–O spinels are not obtained below about 600°C. Alternatively, well crystalline spinels with cationic vacancies can be prepared by soft synthesis routes (2). At 600°C the spinel particle size was about 20–50 nm, and at 850°C it was about 0.2 μm according to broadening X-ray diffraction line (311) and electron micrographs.

X-Ray Powder Diffraction

We found that cubic spinels obtained can be divided into three composition ranges: line A and regions B and C. The ranges are indicated in Figs. 2 and 3. This apparently arbitrary division was useful for further discussion of the experimental results. For example, the spinel-lattice parameters plotted against Fe/(Fe + Mn) seem to fall into certain groups rather than follow a simple common dependence for all Li–Fe–Mn–O spinels.

Line A represents the solid solution of $LiFe^{III}_5O_8$ and hypothetical $LiMn^{III}_5O_8$, which was most systematically studied. We found the range of $0.28 \le Fe/(Fe + Mn) \le 1$ for these spinels obtained at 850°C. Blasse (3) reported the boundaries of the solid solutions $0.2 \le Fe/(Fe + Mn) \le 1$ at 1100°C, and Bonsdorf *et al.* (8) $0.4 \le Fe/(Fe + Mn) \le 1$ at 600 to 900°C in air. The oxides $Li(Fe,Mn)_5O_8$ are very stable and can be easily prepared without a special care. Blasse (3) synthesized these oxides at 1100°C, but Mn^{III} in Li–Fe–Mn–O spinels is stable at temperatures ≤ 900°C, otherwise there is a risk of the formation of Mn^{II} reported by Bonsdorf *et al.* (8). Sano *et al.* (15) obtained stoichiometric

TABLE 2
Results of Rietveld Refinement of Selected Single-Phase Spinel Samples

	Region x (O v 32e)	a/Å	Δ a/Å	R_{Bragg}	R_f	A–O/Å	B–O/Å	$x + 0.125$
$Li_{0.47}Fe_{0.71}Mn_{1.78}O_4$	A	0.26413	8.39248	0.00009	6.64	5.74	2.0224	1.9866	0.38913
$Li_{0.43}Fe_{1.03}Mn_{1.51}O_4$	A	0.26324	8.39939	0.00005	4.10	3.38	2.0112	1.9949	0.38824
$Li_{0.43}Fe_{1.23}Mn_{1.31}O_4$	A	0.26042	8.38884	0.00014	4.07	4.15	1.9678	2.0135	0.38542
$Li_{0.49}Fe_{1.19}Mn_{1.27}O_4$	A	0.26174	8.36851	0.00009	4.99	3.91	1.9820	1.9987	0.38674
$Li_{0.54}Fe_{1.45}Mn_{1.02}O_4$	A	0.26149	8.36576	0.00007	4.65	3.85	1.9777	1.9999	0.38649
$Li_{1.00}Fe_{0.16}Mn_{1.77}O_4$	B	0.26335	8.19547	0.00028	3.47	3.67	1.9639	1.9456	0.38835
$Li_{0.94}Fe_{0.37}Mn_{1.70}O_4$	B	0.26361	8.25895	0.00011	2.72	2.44	1.9828	1.9588	0.38861
$Li_{0.99}Fe_{0.37}Mn_{1.65}O_4$	B	0.26350	8.24580	0.00013	2.75	2.43	1.9781	1.9565	0.38850
$Li_{0.66}Fe_{0.43}Mn_{1.85}O_4$	B	0.26370	8.30870	0.00022	5.48	4.39	1.9961	1.9699	0.38870
$Li_{0.88}Fe_{0.58}Mn_{1.47}O_4$	B	0.26326	8.24474	0.00017	3.19	3.35	1.9744	1.9580	0.38826
$Li_{0.59}Fe_{0.67}Mn_{1.68}O_4$	B	0.26409	8.35058	0.00008	6.26	4.88	2.0118	1.9770	0.38909
$Li_{0.80}Fe_{0.62}Mn_{1.52}O_4$	B	0.26385	8.26215	0.00020	5.05	4.51	1.9878	1.9578	0.38885
$Li_{0.70}Fe_{0.65}Mn_{1.60}O_4$	B	0.26509	8.31609	0.00012	5.61	5.00	2.0179	1.9616	0.39009
$Li_{0.94}Fe_{0.59}Mn_{1.42}O_4$	B	0.26330	8.24400	0.00009	2.10	2.12	1.9748	1.9575	0.38830
$Li_{0.56}Fe_{1.41}Mn_{0.99}O_4$	C	0.26171	8.33860	0.00022	12.80	8.87	1.9745	1.9918	0.38671

spinels with a substantial amount of trivalent Mn at temperature as low as 650°C.

At Fe/(Fe + Mn) > 0.8 a change was observed of the crystal symmetry from $Fd3m$ to $P4_332$ (6, 10).

Contrary to Blasse (3), we found that the Vegard law was valid for this solid solution as demonstrated in Fig. 4: the spinel lattice parameter was linearly proportional to Fe/(Fe + Mn). Due to a small variation of Li/(Fe + Mn) in the spinels of line A the influence of the corresponding member in Eq. [1] can be practically neglected. The cubic structure was preserved even at certain Li-deficiency, when Li/(Fe + Mn) ~ 0.18 and the lattice parameter exceeded 8.38 Å (see the samples on the lower boundary of the spinel area in Fig. 2). Such Li-deficient spinels can be considered solid solutions with $MnFe_2O_4$ (10) or Fe_3O_4 (15).

Contrary to a previous report (3), we found simple linear dependence of the fraction of Li in tetrahedral positions with decreasing Fe content down to Fe/(Fe + Mn) = 0.4. In the $0.28 \le Fe/(Fe + Mn) \le 0.4$ range, all Li was in tetrahedral positions. Bonsdorf *et al.* studied Fe distribution among tetrahedral and octahedral positions in $Li(Mn,Fe)_5O_8$ using Mössbauer spectroscopy under an external magnetic field (8). They found that Fe distribution did not depend on the actual Fe/Mn ratio and corresponded to 41% of total Fe present in tetrahedral positions. With respect to such Fe distribution, Fe and Li (according to results by X-ray diffraction) occupy 87–100% of the tetrahedral positions. This conclusion agrees with the preferential placement of Mn^{III} to

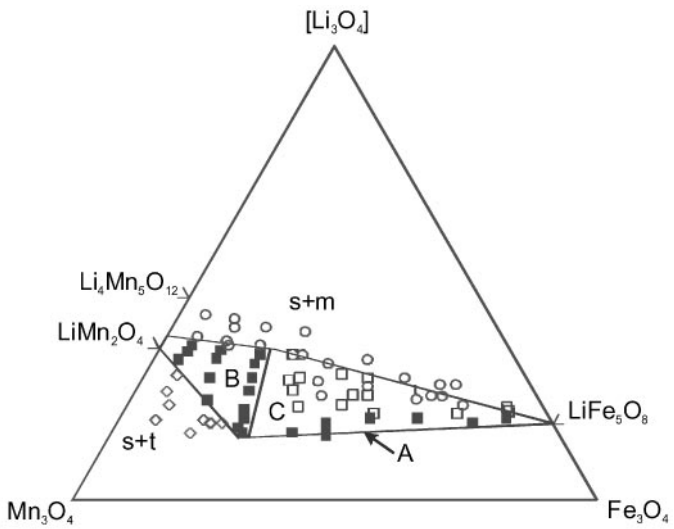

FIG. 2. Composition of the samples studied: (■) single-phase well-crystalline spinels; (□) samples containing two spinels or one spinel and probably amorphous impurity (more details in text); (○) spinel with an admixture of Li_2MnO_3; (◇) spinels with an admixture of tetragonal phases or hausmannite. Abbreviations: s, spinel; m, monoclinic Li_2MnO_3; t, tetragonal phases and hausmannite.

TABLE 3
Regression Analysis of the Relationship between Spinel Lattice Parameter a and Its Elemental Composition According to Eq. [1]

	A/Å	B/Å	C/Å	r
A (n = 11)	8.497(19)	− 0.088(11)	− 0.400(108)	0.973
B (n = 12)	8.460(21)	H0 (P = 92%)	− 0.474(52)	0.945
C (n = 8)	8.417(16)	H0 (P = 42%)	− 0.354(54)	0.938

Note. Standard deviations of the regression parameters are in parentheses; r, regression coefficient; n, number of samples; H0, zero hypothesis accepted on the given significance level P.

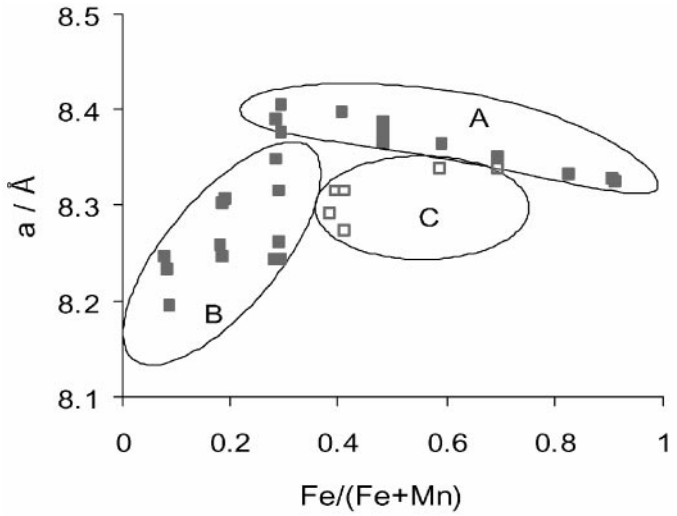

FIG. 3. Lattice parameter of spinels plotted against Fe/(Fe + Mn) ratio. The regions A, B, and C are shown.

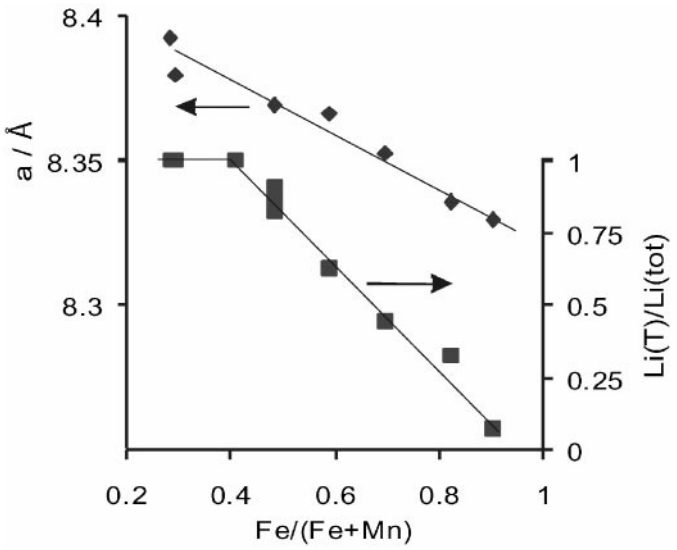

FIG. 4. Lattice parameters and fraction of Li in tetrahedral positions in the spinels of region A.

octahedral positions in $Li(Fe,Mn)_5O_8$ found by Shemyakov *et al.* (7).

Also, in region B, true solid solutions with variable composition $(Li,Fe,Mn)_3O_4$ were obtained. The quadrangular area has the following vertices (in Fig. 2 from top left counterclockwise): $Li_{(1+x)}Mn_{(2-x)}O_4$, $LiMn_2O_4$, $Li(Fe_{0.28}Mn_{0.72})_5O_8$, and $Li_{0.94}Fe_{0.59}Mn_{1.42}O_4$. The easy formation of spinels in region B offers the possibility of synthesizing electrochemical materials of a flexible elemental composition and varying initial Mn valence, which will be examined in future work. The thermal stability of spinels at large Li content depends on temperature. In Fig. 2, the upper boundary of region B was plotted for samples heated at 600°C. Actual maximum valence of Mn in the upper boundary of the region B was 3.7 according to the chemical analysis (Table 1). Assuming only cationic vacancies, the mean occupancy of cationic sites 98% was lower in these spinels as compared to the spinels of line A. At 800 or 850°C, the spinels richest in Li converted to a mixture of Li_2MnO_3 and a Li–Fe–Mn–O spinel depleted in Li. This limited thermal stability of Mn^{IV} under heating in air is well known for Li–Mn–O spinels (1), and there is no reason to expect something else for Li–Fe–Mn–O spinels. Maximum Mn valence ~ 3.9 in well-crystalline Li–Mn–O spinels obtained by ceramic route was found by Le Cras *et al.* at 400 or 600°C depending on the starting compounds, and 850°C was the most suitable temperature to prepare $LiMn_2O_4$ with Mn valence exactly equal to 3.5 (1). From this point of view, the ideal oxygen stoichiometries of the series $Li_4Mn_5O_{12}$–$LiFe_5O_8$ reported by Blasse (3) (obtained by heating at 750°C in oxygen) and formula $Li_2FeMn_3O_8$ of samples for electrochemical studies (12, 18) (obtained at 750°C) were probably not realistic. Li–Mn–O spinels with Mn exclusively in tetravalent state can probably only be obtained by soft synthesis routes (2).

In the spinels of region B, all Li was found in tetrahedral positions. The same was also reported for Li in $Li_2FeMn_3O_8$ (18) $Li_4Mn_5O_{12}$–$LiFe_5O_8$ series at $Fe/(Fe + Mn) \leq 0.27$ (3) and $LiMn_2O_4$–$LiFe_5O_8$ at $Fe/(Fe + Mn) < 0.2$ (4). The lattice parameter was found to be directly proportional to Li/(Fe + Mn) ratio (Fig. 5). Similar dependence of the lattice parameter on Li/Mn ratio was found in Li–Mn–O spinels (1). This dependence is understandable because the actual Li/(Fe + Mn) ratio controls the Mn valence. The actual Fe/(Fe + Mn) ratio has

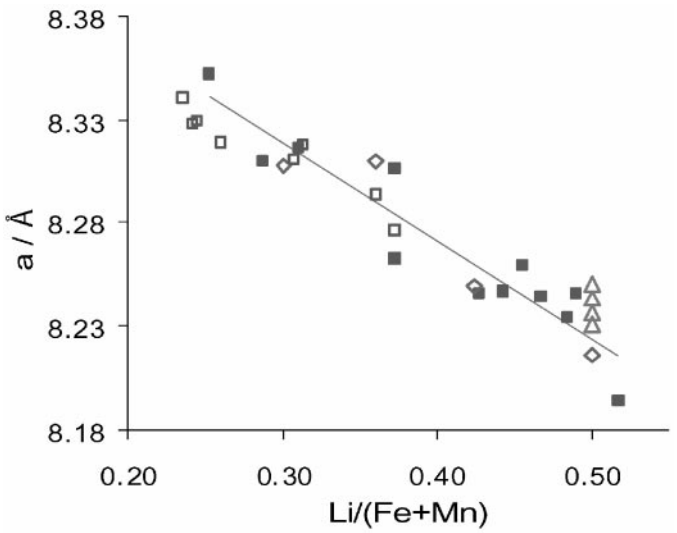

FIG. 5. Lattice parameter of spinels plotted against Li/(Fe + Mn): (■) region B; (□) region C. Data published by (◇) Wolska *et al.* (6) and (△) Song *et al.* (12) are also shown.

a statistically insignificant influence on the lattice parameters (see Table 3), although it was so important in the previous series $Li(Fe,Mn)_5O_8$. We conclude that also in region B uniform solid solution occurs but it has a different properties than the series A.

The samples of region C differed from the previous two groups dramatically. Their formation was much slower under the same temperature and duration of heating, which was sufficient for spinels in the previous two regions. While the spinels of region B were formed in a few hours at 600°C, in region C under the same conditions a pair of spinels arose: one of type A and other of type B. Apparently, the structures of types A and B were preferred to type C at least for kinetic reasons. After heating at 800 or 850°C, the spinels seemed to be single-phase but their X-ray diffraction pattern contained unclear, wide minor lines resembling those of amorphous admixtures. The problems are clearly related to the contradictory temperature requirements: low temperature, suitable to preserve Mn valence above III, is insufficient to finish the synthesis controlled by solid-state diffusion, and higher temperatures 800 or 850°C accelerating the diffusion would tend to decrease the Mn valence to III. Blasse (3) and Wolska *et al.* (4) found deviations of both Vegard law and nontrivial change of Li distribution in the cationic sublattices in the Li–Fe–Mn–O series with Mn valence between III and IV, i.e., in compositional range corresponding to region C. However, the previous authors considered these spinels single phase (3, 4). We are, however, afraid of the possible presence of amorphous impurities indicated by unclear X-ray diffractograms that would deny the actual elemental composition of the remaining well-crystalline spinel. Additionally, Rietveld refinement based on the X-ray diffraction patterns yielded fits with rather poor statistics, as is demonstrated in Table 2 (the last sample), and hence reliable evaluation of the Li distribution was not possible in all cases. Therefore, we searched for further characteristics that would validate our severe evaluation of the sample quality.

Curie Temperature

The reason for determining this numerical characteristic was the result of preliminary (unpublished) study of another series of Li–Fe–Mn–O spinels by Moessbauer spectroscopy. Unfortunately, a difference in hyperfine fields of Fe in tetrahedral and octahedral positions is too low to permit data processing unless an external magnetic field is applied (8), and it is also little sensitive to actual Fe/(Fe + Mn). However, we found that in the room temperature Mossbauer spectra of some samples of region C there are yet apparently noncollapsed sextet (ferrimagnetic ordering) and minor doublet (already paramagnetic phase) as if the spinel was composed of components with two different Curie points (ferrimagnetic to paramagnetic transition). Therefore in this study the temperature dependence of magnetic susceptibility was determined in the spinels with Fe/(Fe + Mn) > 0.38. The Curie temperature, plotted in Fig. 6, was roughly linearly dependent on Fe/(Fe + Mn) ratio for group A in accordance to the finding of Blasse (3).

In about a half of the samples of group C the χ/T curve exhibited more inflex points, i.e., more species with different Curie temperatures. Similar curves were obtained for samples containing more spinel phases according to X-ray powder diffraction. This finding indirectly proved that the unclear shoulders in X-ray powder diffraction patterns of the samples in region C could be attributed to a poorly organized spinel admixture or domains with the elemental composition differing from that of the bulk. An alternative explanation is that the distribution of Fe between tetrahedral and octahedral positions in region C depends significantly on temperature in the temperature range indicated in Fig. 6.

Electrochemical Dissolution in Aqueous Solution

Reductive dissolution of Li–Fe–Mn–O spinels in aqueous solution proceeds as an irreversible reaction

$$\mathrm{Li}_x\mathrm{Fe}_y\mathrm{Mn}_{3-x-y}\mathrm{O}_4(\mathrm{s}) + (2+x)\mathrm{e}^- + 8\mathrm{H}^+ \rightarrow x\mathrm{Li}^+(\mathrm{l}) + y\,\mathrm{Fe}^{2+}(\mathrm{l}) + (3-x-y)\,\mathrm{Mn}^{2+}(\mathrm{l}), \quad [2]$$

where (s) and (l) stand for solid and dissolved species. Electrochemical dissolution of immobilized Fe–Mn mixed oxides was already shown to be very sensitive to Fe/Mn ratio

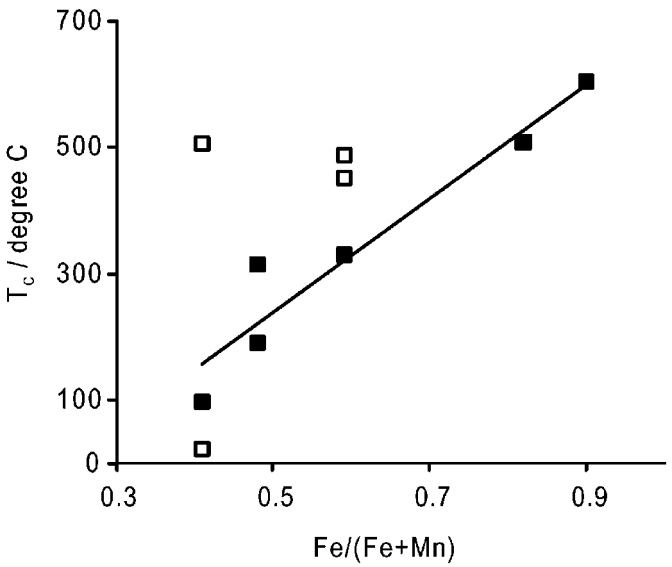

FIG. 6. The Curie temperatures of spinels with Fe/(Fe + Mn) > 0.38: (■) spinels of region A; (□) the spinels of region C, which had a single ferrimagnetic–paramagnetic transition.

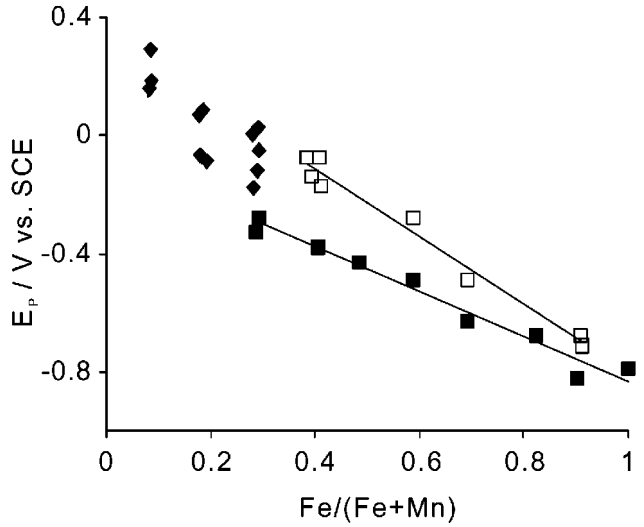

FIG. 7. Peak potentials of the reductive dissolution of Li–Fe–Mn–O spinels plotted against Fe/(Fe + Mn) (■) and regression line (□) spinels of line A with Mn valence 2.95–3.2; (◆) spinels of region B and regression line (□) the spinels of region C with Mn valence 3.4–3.7.

(14, 20). The bigger set of spinels available in the present study permitted us to further specify the influence of the oxide composition on reductive dissolution reactivity of Li–Fe–Mn–O spinels. In Fig. 7, the peak potentials of the spinels studied were plotted against Fe/(Fe + Mn). At Fe/(Fe + Mn) > 0.2 the single-phase spinels yielded simple voltammetric peaks without splitting or shoulders. Some samples with Fe/(Fe + Mn) < 0.2 yielded split peaks suggesting two-step reaction mechanism as it was recently observed for Mn dioxide (22). In this case the potential of the dominant peak was plotted in Fig. 7. At Fe/(Fe + Mn) > 0.2, the voltammetric peak was split exclusively due to bimodal size distribution (one case in spinel A) or probable phase nonuniformity (some spinels in region C). Such heterogeneous samples were omitted in Fig. 7.

The peak potentials vs Fe/(Fe + Mn) yielded a line for the spinels A in accordance with our previous reports (14, 20). The difference in peak potential for the spinels of line A and region C demonstrated a less significant influence of Mn valence. Due to the influence of variable Mn valence, the peak potentials of the spinels of region B occurred in areas of roughly triangular shape, because the peak potential increases not only with decreasing Fe/(Fe + Mn) but also with increasing Li/(Fe + Mn). In previous reports (14, 20) we stated that voltammetry of Li–Fe–Mn–O spinels is more sensitive to Fe/Mn ratio in spinels than to actual Mn valence or particle size, which also contribute to electrochemical reactivity of microcrystalline solids. In this work, we can be more specific: Fe/(Fe + Mn) ratio altered the peak potential within the range of 1.1 V, and Mn valence and particle size was reflected by the scatter of E_P within the range of about 0.3 V at Fe/(Fe + Mn) ~ 0.4, where Li/(Fe + Mn) can be varied in the widest range. Particle size can be responsible for about 0.05–0.1 V difference with the particle size changed by an order of magnitude (29).

Due to such a complex influence of elemental, structural, and granulometric characteristics of spinel samples on their voltammetric peak potential, voltammetry is a sensitive technique to evaluate the quality of synthetic samples. This fact was used for preliminary evaluation of synthetic products before they were submitted to more demanding and time consuming analyses. Under the conditions used, voltammetry took about 5 min and helped us to reveal phase heterogeneity in large sample series. If the synthetic samples contained two species with peak potentials differing by more than about 0.2 V, voltammetry would reveal this heterogeneity. This was frequently the case of biphasic samples, which lie outside the spinel region in Fig. 2. In three samples of the single-phase oxides given in Table 1, one from line A and two from region B, some other heterogeneity was responsible for the splitting or the deformation of the reductive dissolution voltammetric peaks. A subsequent check using TEM showed that these three samples consisted of two kinds of particles: small (tens of nanometers) and large aggregates (~ 0.1 μm in diameter) of coalesced smaller particles.

Voltammetry would hence prove to be an efficient analytical tool complementary to X-ray powder diffraction analysis. From Fig. 3 and 7, the difference in sensitivities of these two methods is apparent: the lattice parameter and hence the position of X-ray diffraction lines are more sensitive to Li/(Fe + Mn) content, whereas electrochemical dissolution reactivity and peak potential are more significantly affected by Fe/(Fe + Mn) ratio.

Electrochemical Li^+ Insertion/Extraction and Mn Valence Cycling in Nonaqueous Solution

The activity for lithium insertion/extraction, well established for Li–Mn–O spinels, is based on reversible oxidation/reduction of trivalent Mn according to Eq. [3],

$$LiMn_2O_4\,(s) \leftrightarrow Li^+\,(l) + e^- + \lambda\text{–}MnO_2\,(s), \qquad [3]$$

where (s) and (l) stand for solid and dissolved species. This electrode process proceeds without destruction of the spinel lattice; the oxidation causes Li^+ extraction and Mn^{3+} oxidation to Mn^{4+} and vice versa provided the supporting electrolyte contains sufficiently high concentration of Li^+ for the back reaction. We restricted the nonaqueous investigation just on the spinels from B region with Fe/(Fe + Mn) lower than 0.3, because it was found that at higher Fe content the Li^+ insertion/extraction is suppressed (12, 20). The spinels selected had Li/(Fe + Mn) between 0.3 and 0.5 and average Mn valence in the 3.58–3.68 range. The

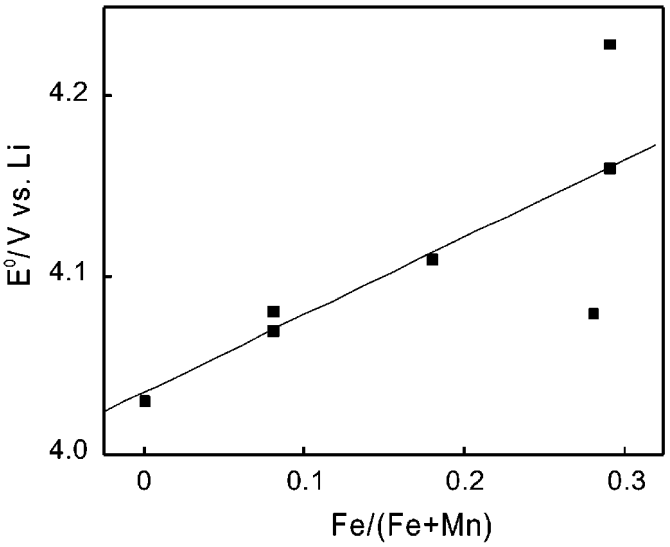

FIG. 8. The dependence of the formal potential of the first Li^+ extraction step in nonaqueous solution on Fe/(Fe + Mn) for selected spinels of region B.

composition of Li–Fe–Mn–O spinels has a pronounced effect on the thermodynamics of the insertion/extraction process. The shift of the formal potential of the first extraction step (see Fig. 8) toward higher values clearly indicates an increase in the spinel stability with an increasing Fe content. We did not observe any pronounced effect of lattice parameters nor Li/(Fe + Mn) on the formal potential. Such observation agrees well with the electrochemical behavior observed by the reductive dissolution, i.e., that the electrochemical behavior is controlled mainly by the iron content.

The literature reports also better capacity retention for Li–Fe–Mn spinels (12), on the other hand our experiments did not indicate such a pronounced effect. The specific capacity, expressed as the ratio of actual to theoretical specific capacity C/C_{teor}, is plotted against Fe/(Fe + Mn) in Fig. 9. C_{teor} was calculated using the stoichimetry of Eq. [3] and assuming the electrochemical cycling of all Mn that was trivalent in the original spinel composition. C/C_{teor} decreases with increasing Fe content in line with the previous finding (12, 20). The amount of the reversibly storable charge ranged between 0.3 and 0.6 of that corresponding to the complete oxidation process. Although the average values of C/C_{teor} seem to be linearly dependent on Fe/(Fe + Mn), a more detailed study is necessary to prove such dependence. We did observe a pronounced increase of anodic charge when cycling to very positive potentials ($E > 4.3$ V). In contrast to Song *et al.* (12) and Kawai *et al.* (18) we did not find any cathodic counter part for this process. A closer investigation of the behavior in this region is, however, necessary to elucidate possible effects of the Li–Fe–Mn structure and those of the electrolyte breakdown at potentials above 4.3 V.

CONCLUSIONS

Under heating in air at 600 to 850°C, $(Li,Fe,Mn)_3O_4$ forms solid solutions in the approximately triangular region of composition $LiFe_5O_8$–$Li(Fe_{0.28}Mn_{0.72})_5O_8$–$LiMn_2O_4$. Rather than a continuous area of solid solutions, we found three regions of similar or continuously changing structural features:

A. $Li(Fe,Mn)_5O_8$ with Fe/(Fe + Mn) > 0.2. Uniform solid solution. Both Fe and Mn are trivalent. Optimal synthesis temperature in air is 850°C. Tetrahedral positions are almost completely occupied by Fe and Li, and the fraction of Li in tetrahedral positions depends linearly on the actual Fe/(Fe + Mn) ratio. The spinel lattice parameter, Curie temperature, and the potential of reductive dissolution depend linearly on Fe/(Fe + Mn).

B. $(Li,Fe,Mn)_3O_4$ with approximate boundaries Fe/(Fe + Mn) < 0.3 and Li/(Fe + Mn) < 0.5. Uniform solid solution. Optimal synthesis temperature is about 600°C (at lower temperatures the spinels are not well crystalline, at higher temperature Mn^{IV} is unstable). Li occupies exclusively tetrahedral positions. Mn valence varies between 3 and 3.7 under heating in air. The Li-excess samples are usually contaminated by Li_2MnO_3. The spinel lattice parameter and potential of reductive dissolution are mainly controlled by Li/(Fe + Mn) (i.e., by Mn valence). The formal potential of the first Li^+ extraction in propylene carbonate depends linearly on Fe/(Fe + Mn).

C. $(Li,Fe,Mn)_3O_4$ with Fe/(Fe + Mn) > 0.4 and Li/(Fe + Mn) > 0.2. Optimal synthesis conditions were not found, spinels arise with difficulties and their elemental uniformity and phase purity is doubtful as follows from

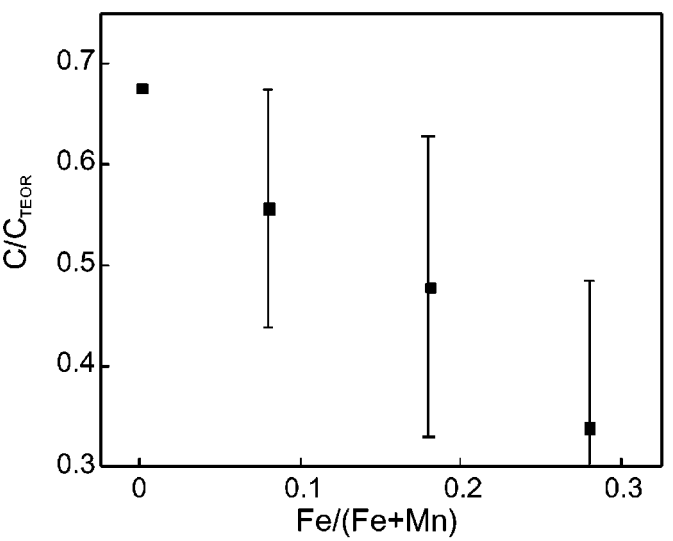

FIG. 9. The dependence of the charge efficiency of Li^+ insertion/extraction reaction on Fe/(Fe + Mn) ratio for selected spinels of region B.

careful examination of X-ray diffraction patterns. Thermal dependence of magnetic susceptibility revealed more species with different Curie temperatures. According to X-ray diffraction, Li is moving to octahedral positions with growing Fe/(Fe + Mn). Available literature data also shows that the solid solutions of Li–Fe–O and Li–Mn–O spinels deviates of the Vegard law and have a nontrivial change of the Li distribution. This non-ideality will probably show that the actual spinel composition and ion occupation will depend on the preparation procedure and is hence hardly reproducible.

ACKNOWLEDGMENT

The authors thank Jan Framberk for elemental and redox analysis of the Li–Fe–Mn–O oxides.

REFERENCES

1. F. Le Cras, P. Strobel, M. Anne, D. Bloch, J.-B. Soupart, and J.-C. Rousche, *Eur. J. Solid State Inorg. Chem.* **33,** 67 (1996).
2. A. Ibarra Palos, M. Anne, and P. Strobel, *J. Solid State Chem.* **160,** 108–117 (2001).
3. G. Blasse, *Philips Res. Repts.* **20,** 528 (1965).
4. E. Wolska, K Stempin, and O. Krasnovska-Hobbs, *Solid State Ionics* **101–103,** 527 (1997).
5. P. Piszora, K. Stempin, and E. Wolska, *Mater. Sci. Forum Vols.* **321–324,** 796 (2000).
6. E. Wolska, P. Piszora, K. Stempin, and C. R. A. Catlow, *J. Alloys Comp.* **286,** 203. (1999).
7. A. A. Shemyakov, A. P. Sefat'evskiy, L. M. Labeznaya, and V. K. Prokopenko, *Neorganicheskie Materialy* **28,** 590 (1992). [in Russian]
8. G. Bonsdorf, K. Schäffer, and H. Langbein, *Eur. J. Solid State Inorg. Chem.* **34,** 1051 (1997).
9. E. Wolska, P. Piszora, J. Darul, and W. Nowicki, *Mater. Sci. Forums*, in print.
10. F. Petit and M. Lenglet, *Solid State Commun.* **86,** 67 (1993).
11. R. F. Gorbanov, R. G. Zakharov, G. N. Orlov, G. I. Chufarov, and A. A. Shchepotkin, *Dokl. Akad. Nauk SSSR* **261,** 633 (1981). [in Russian]
12. M. Y. Song, D. S. Ahn, S. G. Kang, and S. H. Chang, *Solid State Ionics* **111,** 237 (1998).
13. M. A. Zinovik, *Zh. Neroganicheskoi Khimii* **29,** 1811 (1984).
14. T. Grygar, P. Bezdicka, P. Piszora, and E. Wolska, *J. Solid State Electrochem.*, in print.
15. T. Sano and Y. Tamaura, *Mater. Res. Bull.* **34,** 389 (1999).
16. T. Ohzuku, M. Kitagawa, and T. Hirai, *J. Electrochem. Soc.* **137,** 769 (1990).
17. J. M. Tarascon and D. Guyomard, *J. Electrochem. Soc.* **138,** 2864 (1991).
18. H. Kawai, M. Nagata, H. Tukamoto, and A. R. West, *J. Power Sources* **82,** 67 (1999).
19. F. Scholz and B. Meyer, *in* "Electroanalytical Chemistry, A Series of Advances," (A. J. Bard and I. Rubinstein, Eds.), Vol. 20, p. 1. Dekker, New York, 1998.
20. T. Grygar, S. Bakardjieva, P. Bezdicka, and P. Vorm, *Ceramics-Silikáty* **45,** 55 (2001).
21. S. Bakardjieva, P. Bezdička, T. Grygar, and P. Vorm, *J. Solid State Electrochem.* **4,** 306 (2000).
22. A. Doménech-Carbó, M. T. Doménech-Carbó, and L. Osete-Cortina, *Electroanalysis*, in print.
23. D. A. Fiedler, J. O. Besenhard, and M. H. Fooken, *J. Power Sources* **69,** 157 (1997).
24. JCPDS PDF 2 database, Release 50, International Centre for Diffraction Data, Newtown Square, 2000.
25. W. Kraus and G. Nolze, *J. Appl. Crystallogr. Part* 3, **29,** 301 (1996).
26. "Inorganic Crystal Structures Database," FIZ Karlsruhe, release 2000.
27. J. Rodriguez-Carvajal, Fullprof: A program for Rietveld Refinement and Pattern Matching Analysis, *in* "Collected Abstracts of Powder Diffraction Meeting," Toulouse, France, p. 127, 1990.
28. P. Krtil and D. Fattakhova, *J. Solid State Electrochem.* **5,** 196 (2001).
29. T. Grygar, *J. Solid State Electrochem.* **2,** 127 (1998).